J. Fluid Mech. (1992), *vol.* 236, *pp.* 557–577
Printed in Great Britain

Cellular Stokes flow induced by rotation of a cylinder in a closed channel

By MUSTAPHA HELLOU† AND MADELEINE COUTANCEAU
Laboratoire de Mécanique des Fluides, Université de Poitiers, 40, Avenue du Recteur Pineau, 86022 Poitiers, France

(Received 27 March 1991 and in revised form 12 September 1991)

The evolution of the cellular structure of the two-dimensional creeping flow induced by a rotating circular cylinder set in the centre of a rectangular channel is studied numerically and experimentally when the aspect ratio A increases from 1 to 7. In the calculations, depending on the value of A, either only series in terms of polar coordinates, or both matched polar and Cartesian coordinates series are employed to represent the stream function and an efficient least-squares method, very easy to program, is selected to satisfy some of the boundary conditions. For the experiments, a special technique which visualizes intermittently the paths of solid tracers during long times of exposure permits us to observe the fluid motion in the whole domain, even in the regions where the velocities are very small. An excellent measure of agreement between the numerical and experimental results is found. Thus it is clearly shown how, in the region beyond the rotating flow directly driven by the cylinder, the two main corner cells visualized at $A = 1$, develop with increasing A and then coalesce, to finally merge and give rise to a single central cell. This central cell develops in its turn, tending finally to the unbounded channel reference cell, after passing through a maximum length however. Owing to the very high precision of the calculations, many details of thc flow development have been clearly shown, in particular the periodicity, with increasing A, of all the different phases, progressively inducing a succession of cells. The prediction that the angle of separation of the fluid boundaries of the cells tends towards the theoretical limit of 58.61° when the aspect ratio becomes large is also confirmed.

1. Introduction

The literature shows that during the last decade numerous works on creeping flows have been devoted to separation phenomena and to the viscous cells which generally result. This cellular motion interests scientists not only from a fundamental point of view, but also because it is encountered in numerous applications, described for example by Shen & Floryan (1985), Higdon (1985) and Rybicki & Floryan (1987).

By studying the plane flow at a sharp corner, Dean & Montagnon (1949) were the first to find complex exponents in solutions of the Stokes equation, expressed in the polar form, when the angle subtended by the intersecting planes is less than 146° 3′. Fifteen years later, Moffatt (1964) showed that these complex exponents imply the existence of an infinite set of eddies of decreasing size and intensity as the corner is approached. Since then, separation phenomena have been found for variously shaped

† Present address: Laboratoire de Géotechnique, Thermique et Matériaux, Institut National des Sciences Appliquées, 20 Avenue des Buttes de Coësmes, 35043 Rennes, France.

bounding walls and bodies. For example, Sanders, O'Brien & Joseph (1980) again investigated, analytically and numerically, the case examined by Moffatt when the angle between the intersecting planes is 10° and obtained ten successive cells. Collins & Dennis (1976) considered the two-dimensional secondary flow generated by a primary axial flow, under a constant pressure gradient, through a curved tube whose cross-section is a right-angled isosceles triangle. These authors calculated the streamlines of six of the antisymmetric cells which develop in each of the 45° angles of the triangle and those of six of the symmetric cells in the 90° angle. Davis & O'Neill (1977) showed analytically that, in the two-dimensional shear stress flow around a circular cylinder in contact with a plane, an infinite set of eddies is induced in each of the cusps. Moreover, when the cylinder is not exactly in contact with this plane, but at a short distance ϵ less than $0.685a$, where a is the cylinder radius, the flow separates alternately from the cylinder and the plane, forming eddies which interlace as ϵ decreases.

Some of these types of separated Stokes flows with cellular structure have also been observed experimentally. Thus, Taneda (1979) was able to visualize the first two cells in the flow confined by two 28° 5′ intersecting planes and driven by a rotating cylinder at the fluid surface. He also visualized the first viscous cell of the flow studied by Davis & O'Neill (just described above) for $\epsilon = 0.50$, 0.20 and 0. Various other examples may be found in Hasimoto & Sano's (1980) review.

Moffatt suggested that the case of the flow between two intersecting planes leads one logically to consider the limiting case of zero angle, i.e. the case of two parallel boundary planes. In this category, the closed rectangular cavity has been studied most often. Thus, Weiss & Florsheim (1965), Burgraff (1966), Pan & Acrivos (1967), Mehta & Lavan (1969), O'Brien (1972), Shen & Floryan (1985) and Higdon (1985) have all considered the flow induced in rectangular cavities for various values of the aspect ratio h/w, where h and w are the height and the width of the cavity respectively. The sources of motion were a Couette, Poiseuille or Couette–Poiseuille profile. In all cases, a cellular structure develops in the cavity. It consists, according to the value of h/w, either in only small cells located in the cavity corners, usually called Moffatt cells, or in one or several other single cells, i.e. cells centred on the cavity axis. For example, Pan & Acrivos (1967), studying the flow induced by the uniform translation of the top wall, for $h/w = 0.25$, 0.50, 1, 2 and 5, found one single cell for $h/w = 0.25$, 0.50 and 1 which progressively grows as h/w increases; on the other hand, they found two and four single cells for $h/w = 2$ and 5 respectively. In the latter case, the downward fourth cell appears to be strongly influenced by the fixed bottom walls, whereas the structures of the other cells are almost identical, with a length of 1.40 times the cavity width.

The cellular structure of the flow in a rectangular cavity was confirmed experimentally by Taneda (1979) for $h/w = 0.5$, 1 and 2. However, only the first of the two cells which are normally set up in a cavity of aspect ratio 2 has been visualized. More recently, Hellou (1983) and Coutanceau *et al.* (1984), in their investigations of the flow induced by a rotating circular cylinder in a channel of aspect ratio 7 with a 0.50 confining ratio (the cylinder diameter divided by the channel width), have visualized experimentally two oppositely rotating successive cells which occur beyond the main current driven by the cylinder.

When the planes become infinitely large, O'Neill (1983) and Bourot (1984) have shown theoretically that, beyond a certain distance from the source of the motion, the flow consists of an infinity of successive cells, with an antisymmetric behaviour if the source of the motion is not itself symmetrical. The axial dimension of these cells

is 1.40 times the channel width and the angle of separation of their fluid boundary is 58.61°. From now on, they will be taken as a reference cell.

The purpose of the present investigation is, by referring to the flow induced by a rotating cylinder placed in the centre of a rectangular channel, to show how the cellular structure, generated by successive flow separations, develops when the aspect ratio A of the channel increases from a square shape ($A = 1$) to a sufficiently elongated shape ($A = 7$) to render extrapolation to the infinite channel case possible. The confining aspect ratio was maintained at the value of 0.5.

The study is conducted by developing in parallel numerical procedures and a visualization technique. These procedures and the technique are presented in §§2 and 3 respectively, the last section, §4, being devoted to the presentation of the corresponding results and to their comparison. An excellent agreement is found between the numerical and experimental results, and different phases and their periodicity are demonstrated in the flow evolution with increasing A, especially in the development of the corner eddies and in the unexpected consequence of their merging upon the evolution of the length of the preceding central cell.

2. Mathematical formulation and numerical procedure

Let us consider an infinitely long vertical circular cylinder of radius R, placed symmetrically in a horizontal channel of rectangular cross-section, which is limited by two flat endwalls, parallel to each other and normal to the axis of the channel, as shown in figures 1 and 4; $2x_0$ and $2y_0$ are respectively the length and the width of the channel.

This channel is filled with a highly viscous fluid of constant physical properties; its kinematic viscosity is denoted by ν. The motion is obtained by a very slow rotation of the cylinder with a uniform angular velocity ω_0. Thus the Reynolds number of the flow, defined by $Re = (\omega_0 R^2)/\nu$, is supposed to be sufficiently small to ensure the validity of the Stokes regime hypothesis. Under these conditions, the equation of motion in the horizontal cross-section is

$$\nabla^2(\nabla^2 \Psi) = 0, \tag{1}$$

where Ψ is the stream function and ∇^2 a second-order differential operator.

The solution of (1), expressed in polar coordinates, was given by Bouard (1983) and Bouard & Coutanceau (1986) in the form

$$\begin{aligned}\Psi = {} & a_0 + b_0 \log r + c_0 r^2 + d_0 r^2 \log r \\ & + (a_1 r_1^{-1} + b_1 r \log r + c_1 r + d_1 r^3) \cos\theta \\ & + a_1' r^{-1} + b_1' r \log r + c_1' r + d_1' r^3) \sin\theta \\ & + \sum_{n=2,3\ldots}^{\infty} (a_n r^{-n} + b_n r^{-n+2} + c_n r^n + d_n r^{n+2}) \cos n\theta \\ & + \sum_{n=2,3\ldots}^{\infty} (a_n' r^{-n} + b_n' r^{-n+2} + c_n' r^n + d_n' r^{n+2}) \sin n\theta, \end{aligned} \tag{2}$$

where $a_n, b_n \ldots$ are arbitrary coefficients to be determined by the boundary conditions. In our case, if the coordinate r and the radial and the tangential velocity components V_r and V_θ are normalized by R and $\omega_0 R$ respectively, these conditions are

no slip on the cylinder: $\qquad V_r = 0, \quad V_\theta = 1;$

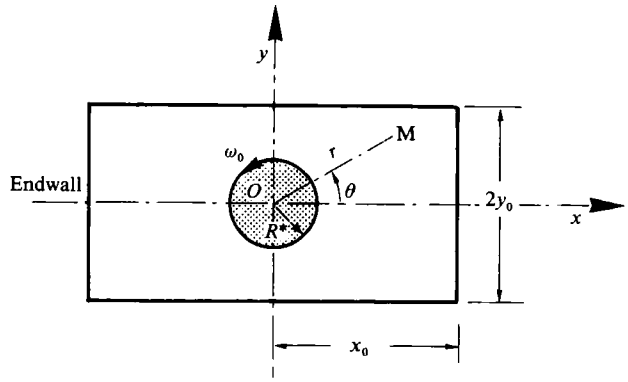

FIGURE 1. Coordinate frames related to the channel and cylinder respectively.

no slip on the channel walls: $V_r = V_\theta = 0$;

and the conditions related to the antisymmetric behaviour of the flow:

$$\Psi(r,\theta) = \Psi(r,\pi-\theta), \quad \Psi(r,\theta) = \Psi(r,-\theta).$$

Applying the symmetry condition and the no-slip condition on the cylinder to (2), we obtain

$$\Psi = a_0 - \tfrac{1}{2}r^2 + b_0(\log r - \tfrac{1}{2}r^2) + \sum_{n=2,4,6}^{\infty}\left[\left(\frac{1-n}{n}r^{-n} + r^{-n+2} - \frac{r^n}{n}\right)b_n + \left(\frac{r^{-n}}{n} - \frac{n+1}{n}r^n + r^{n+2}\right)d_n\right]\cos n\theta, \quad (3)$$

where n is an even integer because of the antisymmetry of the flow. For convenience, we impose $\Psi = 0$ on the channel walls; thus the constant a_0 is expressed as a function of b_n, d_n and y_0. Note that b_0 represents the ratio of the torque experienced by the cylinder in the channel to the torque experienced by this cylinder in an infinite medium; thus b_0 is a measure of the global confining effect.

As opposed to the no-slip condition on the cylinder, which is satisfied exactly by the polar coordinate series (3), the no-slip condition on the channel walls cannot be satisfied exactly by these series because these walls are not coordinate surfaces of the frame that we have used to define the stream function. Thus, this latter condition has been satisfied optimally by using a numerical method. For this purpose, the quadratic minimization method proposed by Bourot (1969) to resolve the satisfaction of the boundary conditions has been used. The efficiency of this method, which is easy to program, has often been proved, for example in the recent works of Coutanceau & Thizon (1981), Maalouf & Bouard (1986), Bourot & Moreau (1987). This method consists of minimizing the quadratic difference between the imposed velocity on the boundary and the velocity deduced from the series (3), which may be written in the form

$$\frac{\partial}{\partial A_i}\int_\Gamma V^2\,\mathrm{d}s = 0, \quad i = 1,2,\ldots,2N+1,$$

where A_i represents the coefficients b_0, b_n and d_n, N the number of terms retained in the series (3) and Γ is the outer boundary, limited here to a quarter of the channel boundary because of the symmetry of the problem, see figure 2. Indeed, for

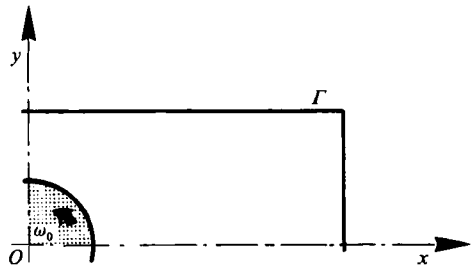

FIGURE 2. Outer boundary retained for the calculations.

Aspect ratio	Velocity
1.0	5.4×10^{-7}
1.5	1.6×10^{-7}
2.0	1.7×10^{-7}
2.5	5.4×10^{-7}
3.0	2.4×10^{-6}
3.5	9.6×10^{-6}

TABLE 1. The mean values of the velocity on the channel walls

convenience of programming, we can write the expressions for the velocity components, calculated from the stream function (3), in the linear form

$$V_r = \sum_j A_j F_j, \qquad j = 1, 2, \ldots, 2N+1,$$

$$V_\theta = r + \sum_j A_j G_j, \quad j = 1, 2, \ldots, 2N+1.$$

Then the minimization yields the linear system

$$\sum_j A_j \sum_{N_P} (F_i F_j + G_i G_j) = -r \sum_{N_P} G_i, \quad i = j = 1, 2, \ldots, 2N+1.$$

In this system, the integrals are replaced by a simple summation on an adequate number N_P of points, regularly spaced on the boundary Γ, which must be at least 2.5 times the number of coefficients (see Sigli 1970).

In our calculations, the limiting value of the accuracy tolerance was fixed at 10^{-6}. This value is of the order of the velocity in the farthest cell for the largest aspect ratio studied here, i.e. $A = 7$. Thus, using 61 coefficients of the series and 181 minimization points, we have obtained excellent accuracy for aspect ratio A up to 3, see table 1.

However, beyond $A = 3$, this accuracy becomes insufficient to detect clearly the cellular flow near the endwalls. The increase of the error is due to the presence of the positive exponents in the series which increase with increasing distance. To solve this problem, we have introduced, in addition to the polar coordinate series, Cartesian coordinate series expansions, which satisfy exactly the no-slip condition on the longitudinal channel walls. These series expansions were given by Bourot (1984), for antisymmetric flow, in the form

$$\Psi(x, y) = \sum_{n=1,2}^{\infty} e^{\lambda_n x} \{A_n (P_n \cos \mu_n x - Q_n \sin \mu_n x) + B_n (P_n \sin \mu_n x + Q_n \cos \mu_n x)\}$$
$$+ e^{-\lambda_n x} \{C_n (P_n \cos \mu_n x + Q_n \sin \mu_n x) + D_n (P_n \sin \mu_n x - Q_n \cos \mu_n x)\}, \quad (4)$$

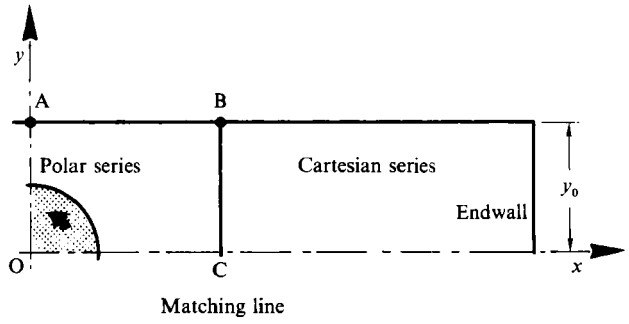

FIGURE 3. Delineation of the domains where the polar and Cartesian coordinate series are used.

	$\frac{\Delta V}{V}$	$\frac{\Delta P}{P}$	$\frac{\Delta \zeta}{\zeta}$	V	V
A	Matching line			Lateral wall	Endwall
4	2.1×10^{-7}	2.6×10^{-8}	4.3×10^{-8}	1.5×10^{-9}	2.9×10^{-7}
5	2.5×10^{-8}	2.8×10^{-9}	4.9×10^{-9}	4.3×10^{-10}	5.8×10^{-8}
6	8.1×10^{-8}	1.1×10^{-9}	2.4×10^{-9}	3.2×10^{-10}	1.5×10^{-8}
7	8.4×10^{-9}	1.2×10^{-9}	2.3×10^{-9}	3.2×10^{-10}	1.1×10^{-9}

TABLE 2. Test showing the accuracy of the calculation from the verification of the matching and no-slip condition; V, P, ζ are the velocity, pressure and vorticity respectively.

with

$$2P_n = (y_0-y)\{\sin\lambda_n(y_0+y)\cosh\mu_n(y_0+y)\}+(y_0+y)\{\sin\lambda_n(y_0-y)\cosh\mu_n(y_0-y)\},$$
$$2Q_n = (y_0-y)\{\cosh\lambda_n(y_0+y)\sinh\mu_n(y_0+y)\}+(y_0+y)\{\cos\lambda_n(y_0-y)\sinh\mu_n(y_0-y)\},$$

and λ_n and μ_n solutions of the complex equation

$$\sin 2a_n y_0 = -2a_n y_0, \quad a_n = \lambda_n + \mathrm{i}\mu_n. \tag{5}$$

For more information about the properties of the corresponding expansion functions of (4) (also encountered frequently in the solution of elasticity problems (Buchwald 1964) and known as Papkovich–Fadle functions), see Joseph & Sturges (1975), Bourot (1984), Moreau (1985). Here we refer to the values given by Moreau with 32 digits for the real and imaginary parts of a_n ($n = 1$–6) and for the corresponding length and intensity ratio between two successive cells of the same range.

When the aspect ratio is greater than 3, we have matched the polar coordinate series (3) and the Cartesian coordinate series (4), satisfying the no-slip condition on the cylinder and on the lateral walls respectively, so that the following conditions remain to be verified: the no-slip condition on part AB of the wall, with the polar coordinate series, see figure 3; the no-slip condition on the endwall, with the Cartesian coordinate series; the matching of the two series to ensure the continuity of the velocity and of the stress.

The matching of the series was done, using again the least-squares method, on a straight line positioned at $x = 1.5y_0$; this position, was selected not too far from the cylinder but beyond the extent of the main rotating flow. In this way, we have

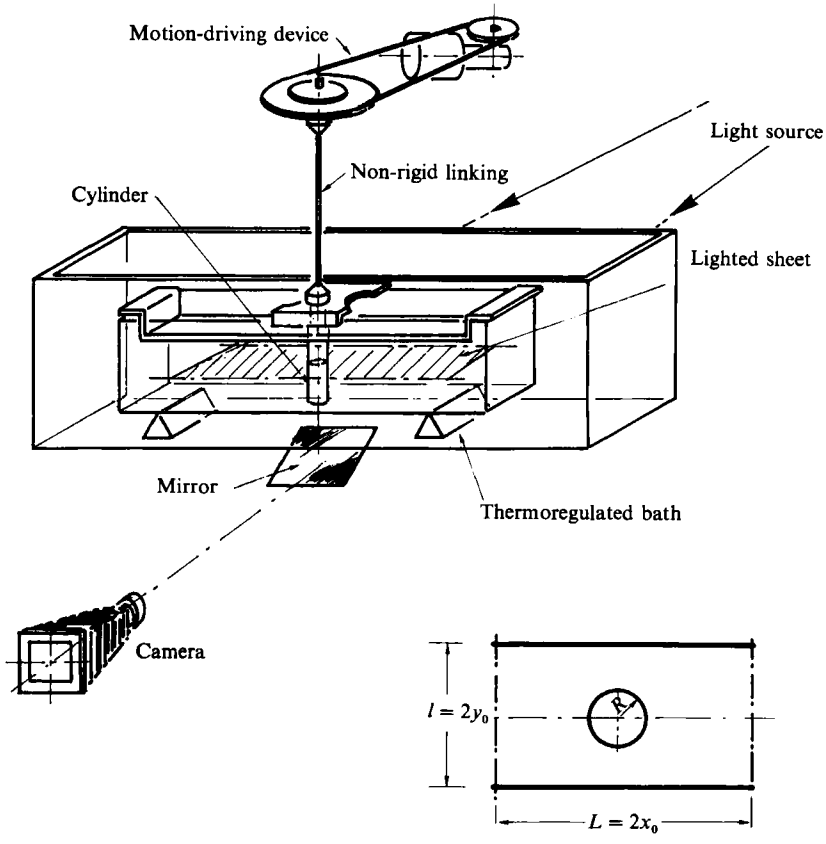

FIGURE 4. Sketch of the experimental apparatus.

obtained excellent results for A greater than 3, as shown in table 2 for the velocity V, pressure P, and vorticity ζ.

3. Experimental technique

Figure 4 shows a sketch of the apparatus constructed to visualize the flow. The Altuglass tank with a parallelepiped shape of 28 cm in length, 4 cm in width and 10 cm in height is filled with a highly viscous silicon oil of viscosity 300 P. The motion is obtained by the uniform rotation of a circular cylinder of 2 cm in diameter and 16 cm in length positioned vertically in the middle part of the channel; the rotation speed is $\omega_0 = 3.7$ r.p.m. Thus the Reynolds number is about 0.001. Adjustable flat walls are positioned normally to the channel axis at the same distance on both sides of the cylinder. The visualization is carried out using very small cuttings of magnesium of about 40 μm in length and 4 μm in thickness. They remain in suspension for several weeks and even months as their settling speed remains quite negligible. They are illuminated by a horizontal thin sheet of light coming from an halogen lamp device.

Given that the velocities decrease exponentially along the channel axis, very long times of exposure are required to visualize the flow in the whole domain, particularly for observing the small particle displacements near the endwalls, and for the high aspect ratios. Consequently, it was necessary to take extreme precautions for reducing to a minimum the disturbing currents, especially the natural convection

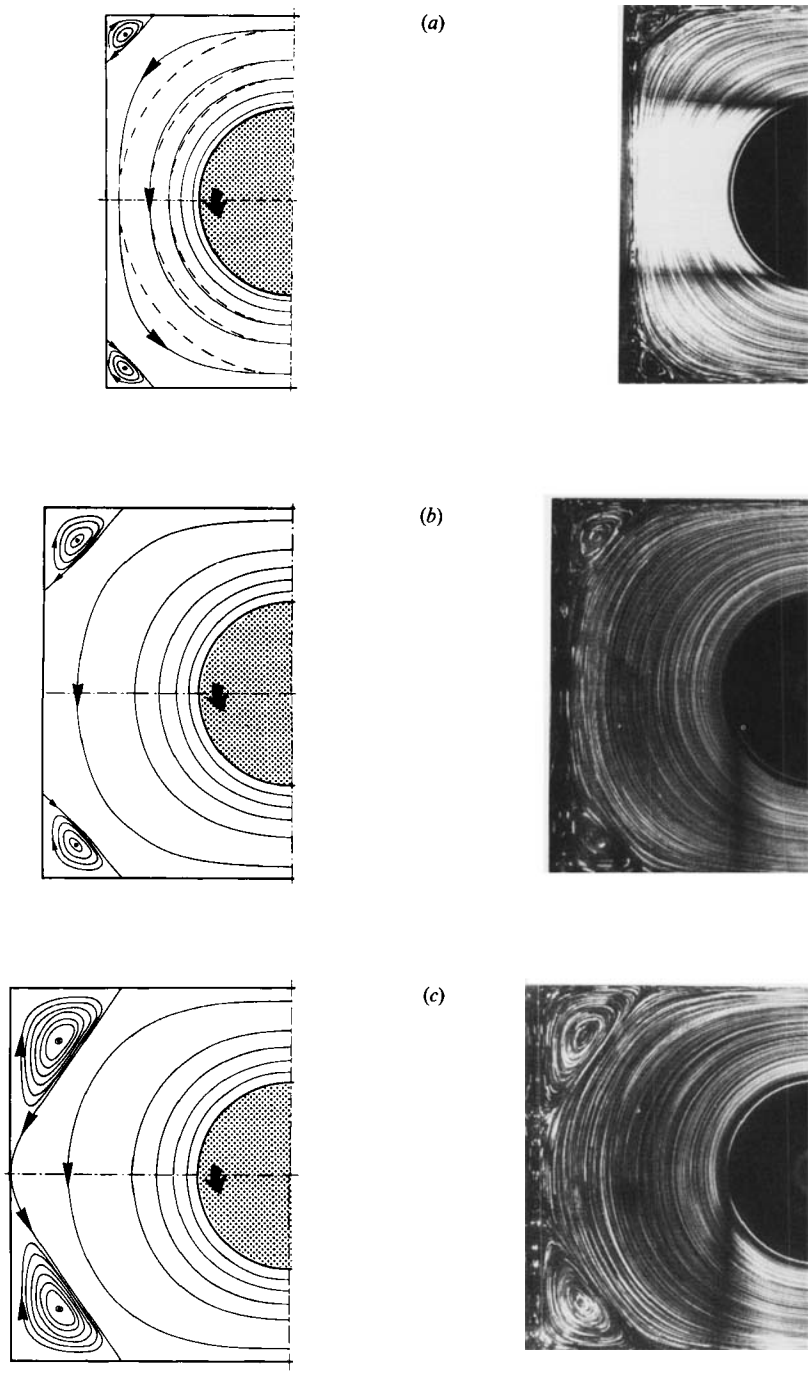

FIGURE 5. Evolution of the structure of the first corner cell: (a) $A = 1$, (b) $A = 1.33$, (c) $A = 1.50$.

currents, which are liable to change completely the phenomena studied. This difficulty has been overcome by the use of a highly viscous oil associated with a suitable rotating speed of the cylinder, ensuring both very low Reynolds number and Newtonian behaviour of the liquid. Furthermore, the channel is fixed in a

thermoregulated bath and intermittent lighting (every 10 s) was used to avoid overheating the fluid; this technique of intermittent exposure was used for A greater than 3. Moreover, it appears necessary to position the cylinder with great precision to avoid transverse velocities and consequently streamlines that are not closed.

4. Numerical and experimental results

Let us now compare our experimental and numerical results on the process of formation of the first and the second single cells. For this purpose, parallel presentation of the calculated streamline patterns and the visualization pictures are given in figures 5–7, 11 and 12.

4.1. *Formation process of the first single-core cell*

For $A = 1$, the flow pattern, which is displayed in figure 5(*a*), shows that the streamlines of the main flow, i.e. the flow directly driven by the rotation of the cylinder, are quasi-circular near the cylinder but tend towards the shape of the channel walls when close to them; for comparison, broken circular lines have been also plotted. Moreover, in each corner, a cell of triangular shape, centred on the diagonal of the cross-section considered, is observed. This cell is in fact the first of the infinity of Moffatt corner cells which we know to exist (Moffatt 1964). We notice the excellent agreement between our numerical and our experimental results. Indeed this good agreement has been obtained for all the aspect ratios studied in this work. Furthermore, for this case of $A = 1$, there is very good agreement with the results of Lewis (1979) obtained for $Re = 1$, both for the streamline pattern and the equi-vorticity pattern (see Hellou 1988) showing that, in these confining wall conditions, inertia interaction is not yet significant.

If we keep the same confining aspect ratio (0.50), it is seen from figures 5(*b*) and 5(*c*), that when the aspect ratio increases from 1 to 1.50, the corner eddies grow progressively larger and the two dividing streamlines which separate them from the main rotating current, come into contact. This leads, at about $A = 1.50$, to the formation of a continuous dividing streamline touching the middle of endwall. As soon as A increases beyond 1.50, this streamline detaches from the endwall and consequently the two corner eddies come into contact by means of a saddle point, see figure 6. This is the start of the process of the coalescing of these eddies, which becomes effective at $A = 1.80$, leading to the formation of the first single-core cell; the photos and streamlines in figure 6(*b–f*) have been selected to show precisely the different phases of this process.

The evolution of the single-core cell as a function of A is presented in figure 7(*a–g*). By examining the streamline patterns associated with the visualization pictures, we see that, when A increases from 1.81 to 4, this cell grows in its turn, becoming more and more stretched towards the endwalls. Furthermore, for $A = 4$, the presence of a new pair of corner cells is clearly seen. These corner cells exist in fact at the previous aspect ratios, but they are much too small and too weak to be visualized. However, our calculations are sufficiently precise to detect them and show that the evolution of their size becomes relevant only beyond A about 3.8. Consequently, the process of formation of a second single-core cell begins to be active from this stage. However it is important to note that the evolution of the first single-core cell is not yet complete.

Some similar configurations to those presented in figures 5–7 were found numerically by Shen & Floryan (1985) and experimentally by Taneda (1979) in the case of the flow induced in rectangular cavities by an external shear flow. These

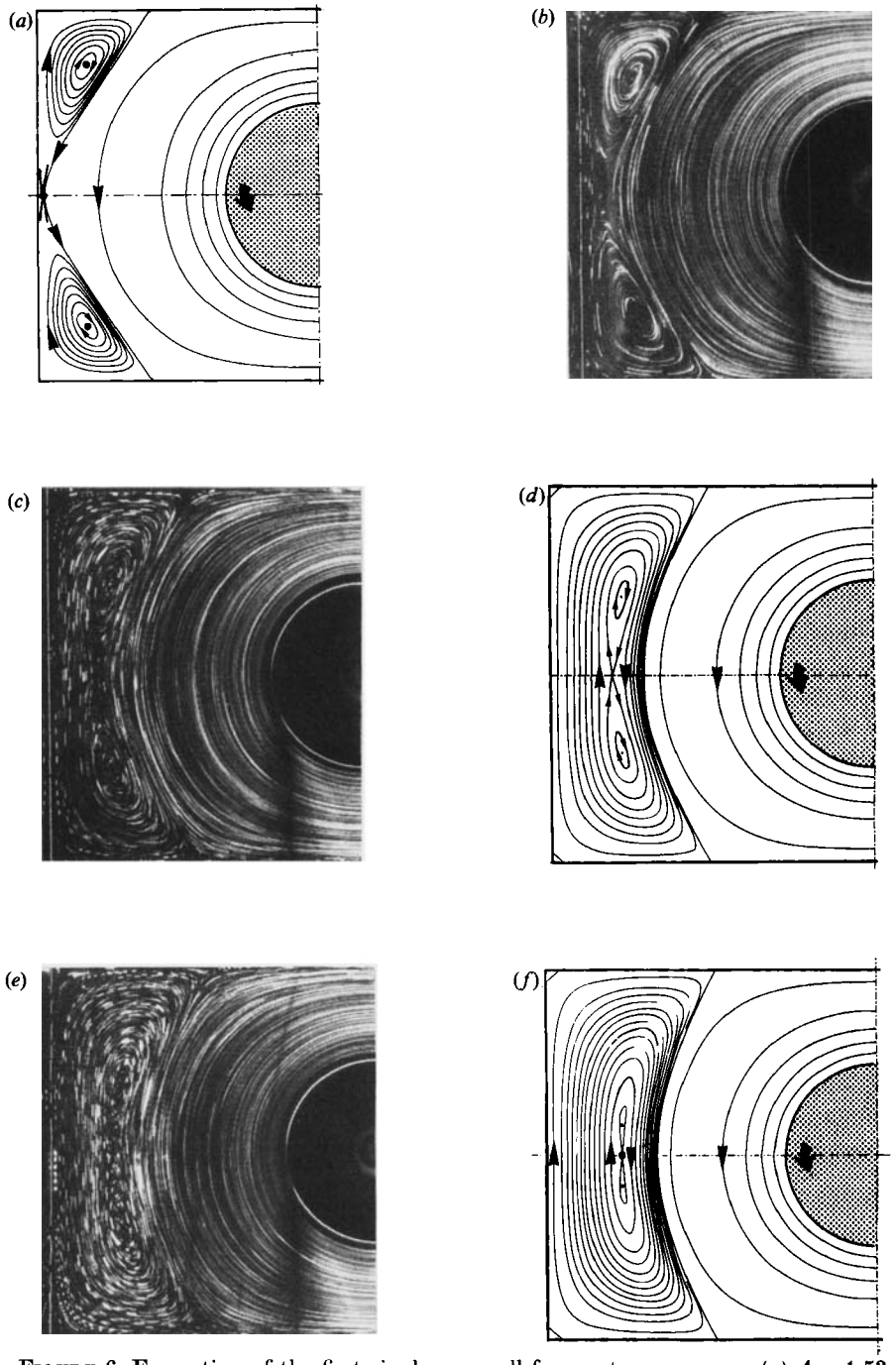

FIGURE 6. Formation of the first single-core cell from a two-core one: (*a*) $A = 1.53$; (*b*) $A = 1.58$; (*c*) $A = 1.68$; (*d*) $A = 1.72$; (*e*) $A = 1.77$; (*f*) $A = 1.79$.

authors have also found that the formation of a single cell starts from the corners. However, they did not give either the details of the corresponding process or the quantitative evolution of the geometrical features of the cells, which we propose to do now.

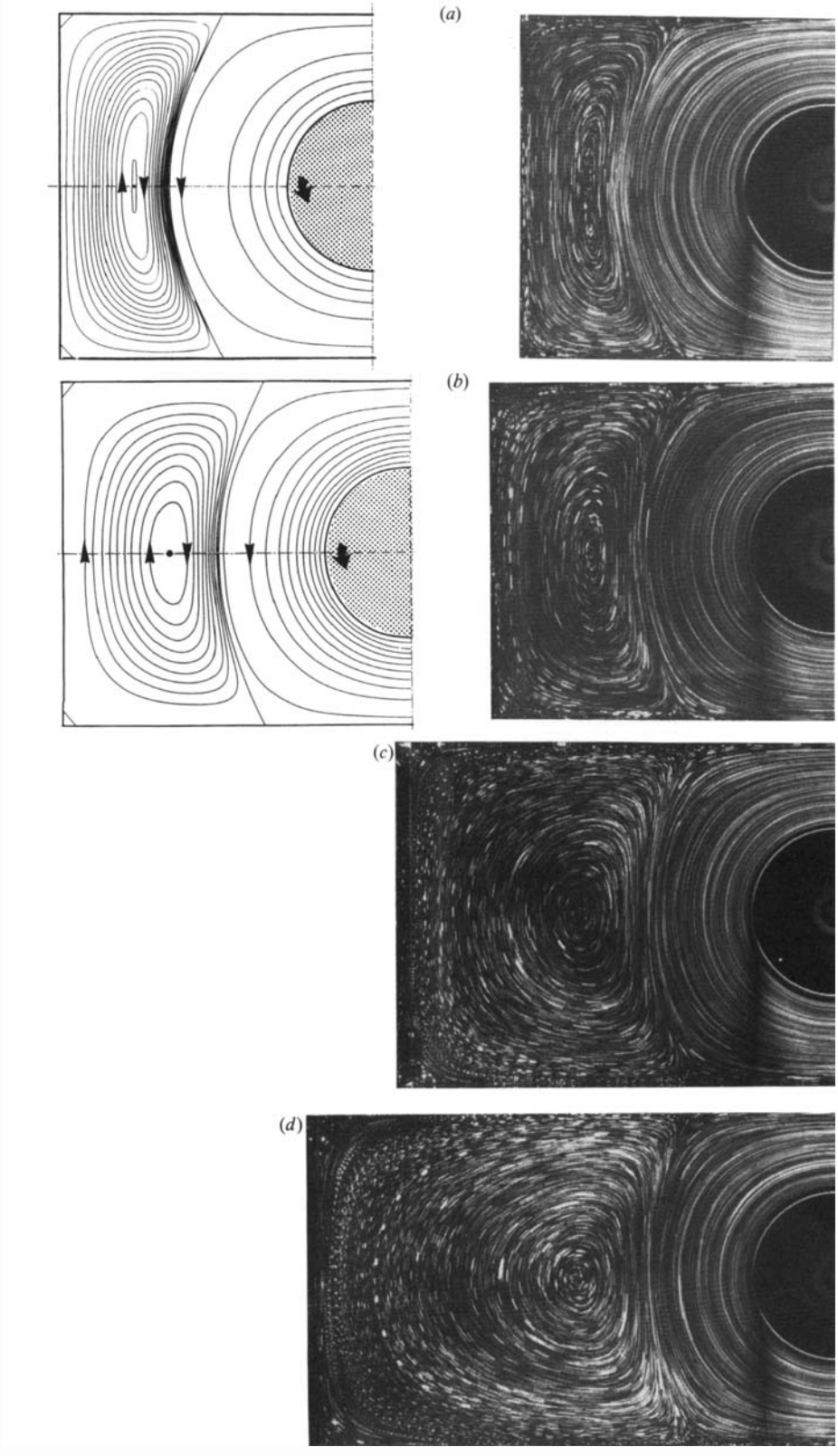

FIGURE 7 (*a–d*). For caption see page 569.

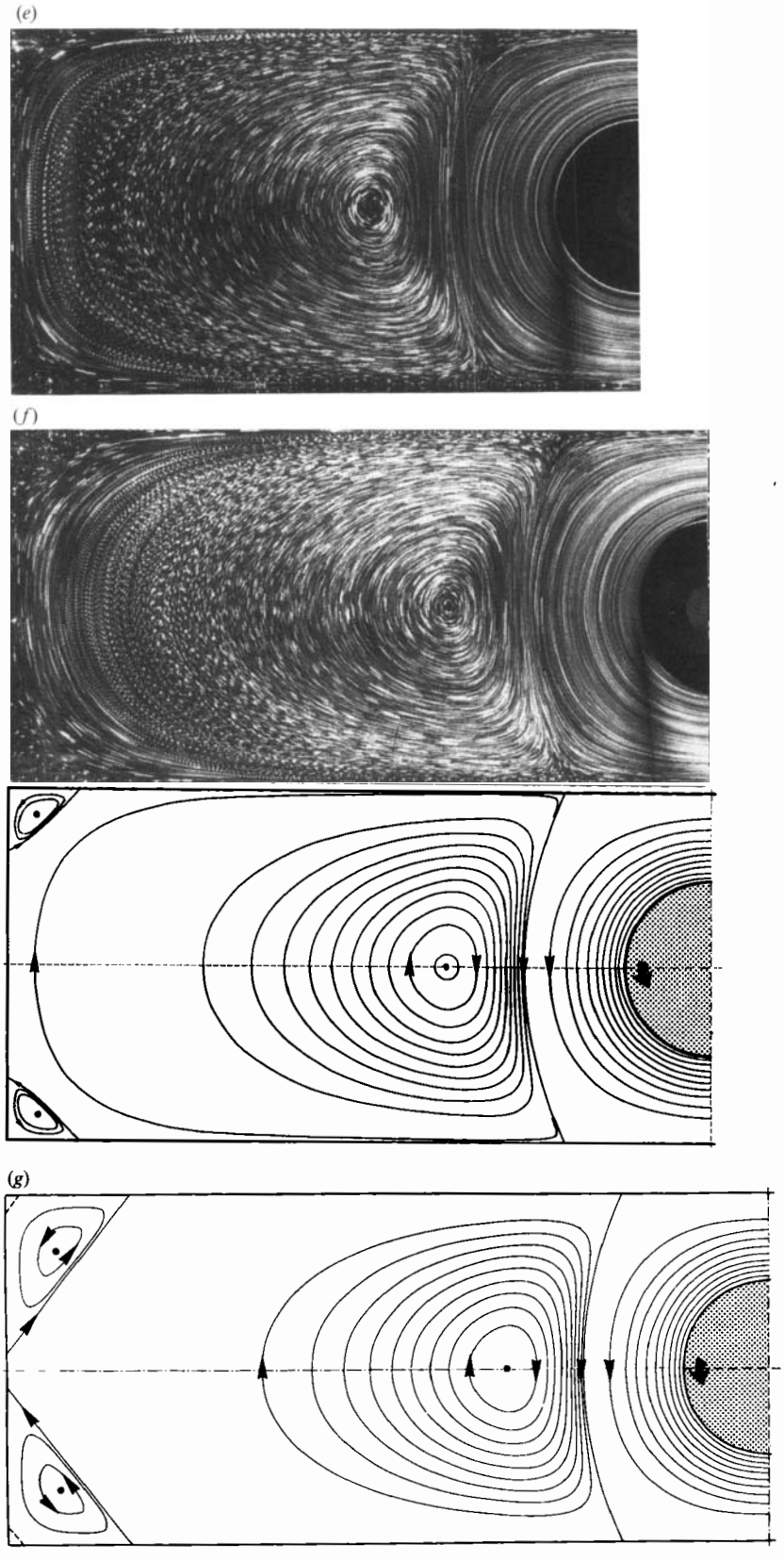

FIGURE 7 (*e–g*). For caption see facing page.

4.2. *Evolution of some typical flow characteristics during the formation of the first single-core cell*

In order to characterize the structure of the flow during the formation of the first single-core cell and its evolution with increasing aspect ratio of the channel, we plot, in figure 8, curves (*a*) and (*b*) showing the evolution of the lengths of the sides L_{S1} and L_{R1} of the first corner cell. It is seen that L_{S1} and L_{R1} grow similarly for A up to about 1.30. When A exceeds this value, the transverse growth of the cell clearly accelerates compared with the lateral growth. In fact, from $A = 1.40$, the displacement of the separation point S_1 corresponds to the endwall displacement itself and, at $A = 1.50$, the reattachment point R_1 reaches the channel axis.

Figure 9 presents the evolution with A of the intersection I_1 (I_1 is defined on figure 10*a*) of the first dividing streamline with the channel axis; the broken line corresponds to the location of the endwall of the channel. It is confirmed that the dividing streamline, which delineates the main driving rotating current, detaches from the endwall at $A = 1.50$, then moves towards the cylinder and, for $A = 2.80$, reaches a limiting location at a distance of $1.07y_0$ from the origin O. Consequently, from this stage, the domain occupied by the main rotating current becomes confined approximately to a square region.

The data are completed by the evolution of the axial stagnation point C_1 (in figure 10*b*) and that of the corner vortex core C'_{11} (in figure 10*c*) during the process of coalescing (A increases from 1 to 1.8); C_1 and C'_{11} are defined on figure 10(*a*). A new phenomenon appears, namely that during the coalescing of the two corner cells, the stagnation point C_1, which is still a saddle point at this stage, is thrown back rapidly towards the cylinder, while the two corner vortex cores approach each other to merge with C_1 into a single point at $A = 1.80$. With further increase of A, C_1 moves off towards the endwall and reaches a limiting position at a distance of $1.51y_0$ from the origin. Consequently, we conclude that the complete merger of the corner cells occurs when the distance of the stagnation point from the cylinder is at a minimum. Taking into account the fact that we have chosen a very large scale to show the phenomena clearly and that the experimental measurements are made within a measure of uncertainty, the agreement between the experimental and numerical data is very good.

4.3. *Process of formation of the subsequent single-core cells*

The new main corner cells, shown for $A = 4$ in figure 7, grow progressively larger and begin to coalesce at $A \approx 4.34$, as clearly shown in figure 11(*a*, *b*). With a further increase of A, we proceed to the formation of a second single-core cell, which grows in its turn, as seen in figure 12(*a*, *b*). Note the still excellent agreement between the calculations and the visualization pictures, particularly for the aspect ratios 5 and 7 for which the visualization was extremely difficult to realize, especially because of the very rapid decrease of the velocity as we move away from the cylinder, as explained before. The flow photographs, obtained by intermittent exposures of 10 s during two hours, illustrate clearly the velocity ratios in the cell field. For example, when the first cell touches the driving rotating current, a fluid particle describes a long trace during each 10 s exposure while, in at the other end of this cell, only a point appears during this time. In the second cell, the particle traces correspond to the two hours exposure!

FIGURE 7. Evolution of the structure of the first single-core cell and the accompanying new corner cells: (*a*) $A = 1.81$; (*b*) $A = 2.02$; (*c*) $A = 2.51$; (*d*) $A = 3.05$; (*e*) $A = 3.59$; (*f*) $A = 4$; (*g*) $A = 4.30$.

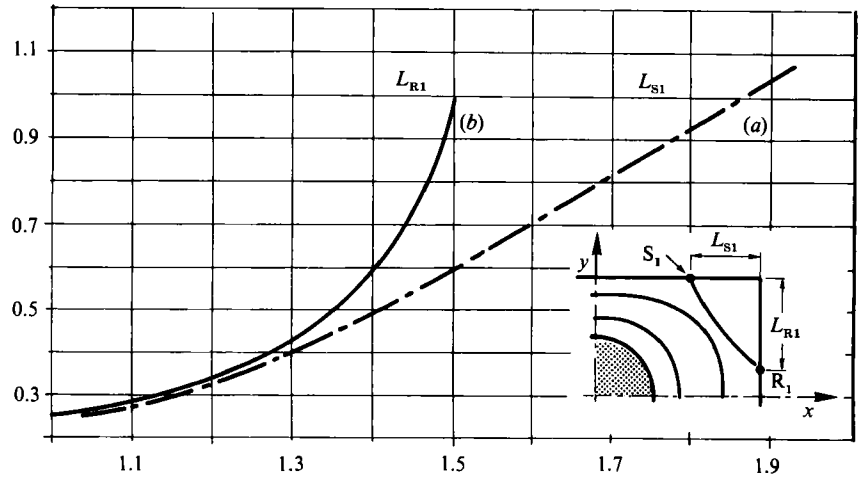

FIGURE 8. Evolution of the lengths of the sides of the first corner cell as a function of the aspect ratio of the channel: (*a*) in the lateral direction; (*b*) in the transverse direction.

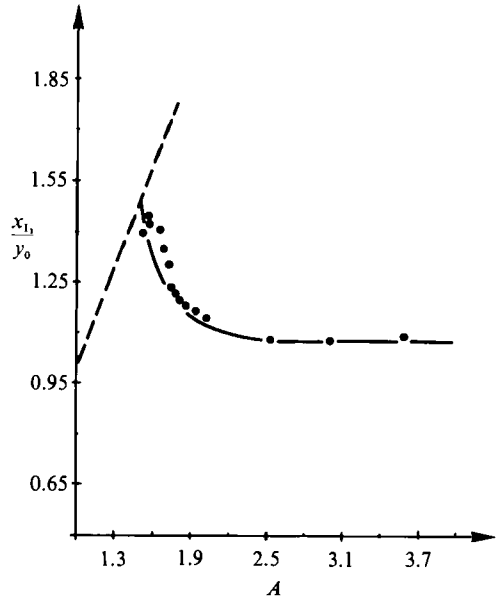

FIGURE 9. Evolution of the intersection I_1 of the first dividing streamline with the channel axis as a function of the aspect ratio A: ——, numerical results; ●, experimental results; ----, location of the endwall.

As we have shown in §4.2, the flow structure is clarified by means of the evolution of some flow characteristics. Thus, figures 13 and 14 show the evolution of the intersection I_2 of the second dividing streamline with the channel axis, and of the second stagnation point C_2 respectively. Similar patterns to those described for I_1 and C_1 are found again, showing the periodic character of the evolution. This periodicity is also illustrated in figure 15, which presents in parallel the evolution of the length of the two single-core cells. It is interesting to note that during the development of the second cell, the length of the first cell contracts from its maximum value of $3.27y_0$, which is reached when the new coalescing process begins,

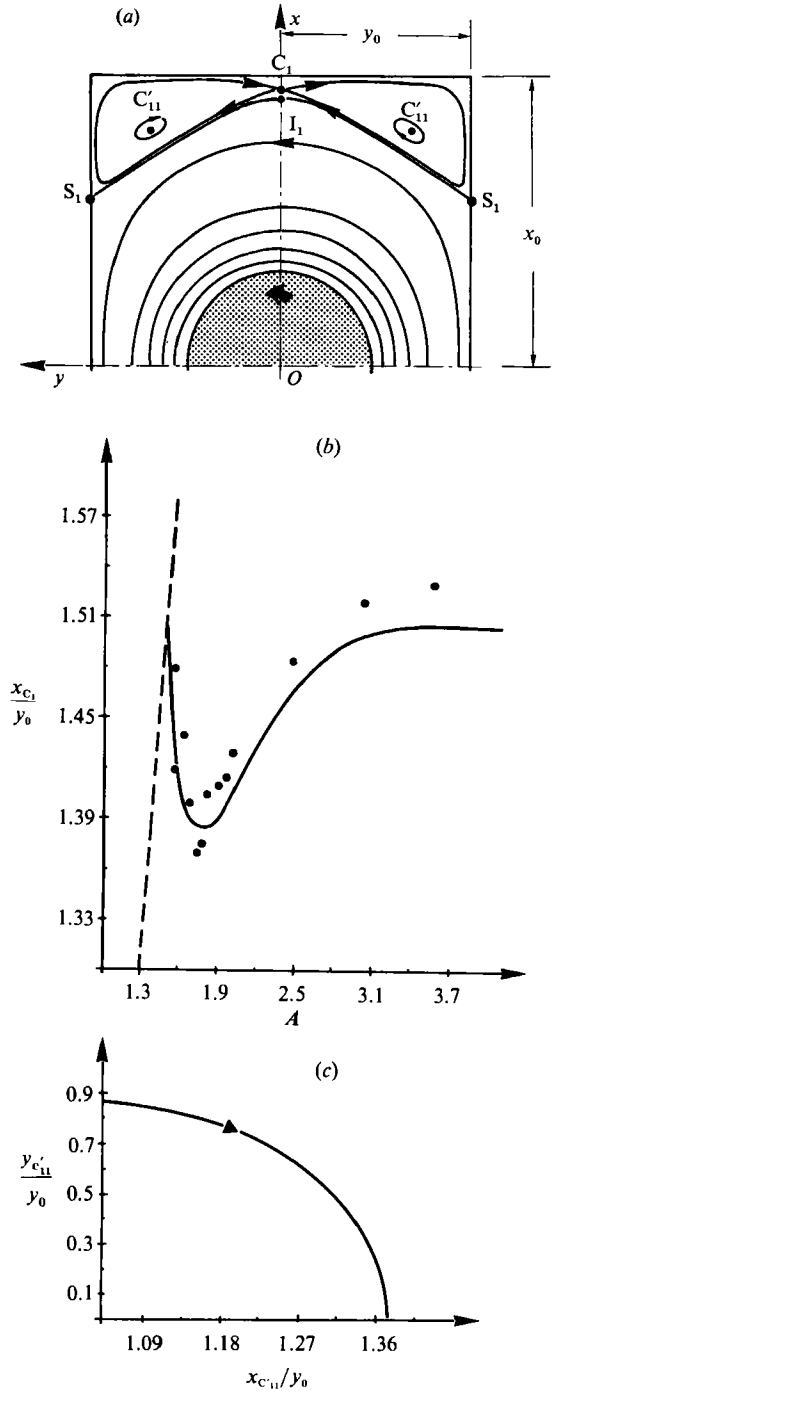

FIGURE 10. (*a*) Notation. (*b*) Evolution, as a function of the channel aspect ratio, of the axial stagnation point C_1 of the first cell: ——, numerical results; ●, experimental results; ----, location of the endwall. (*c*) Trajectory of the centre C'_{11} of the corner cell during the coalescing process (A increases from 1 to 1.80).

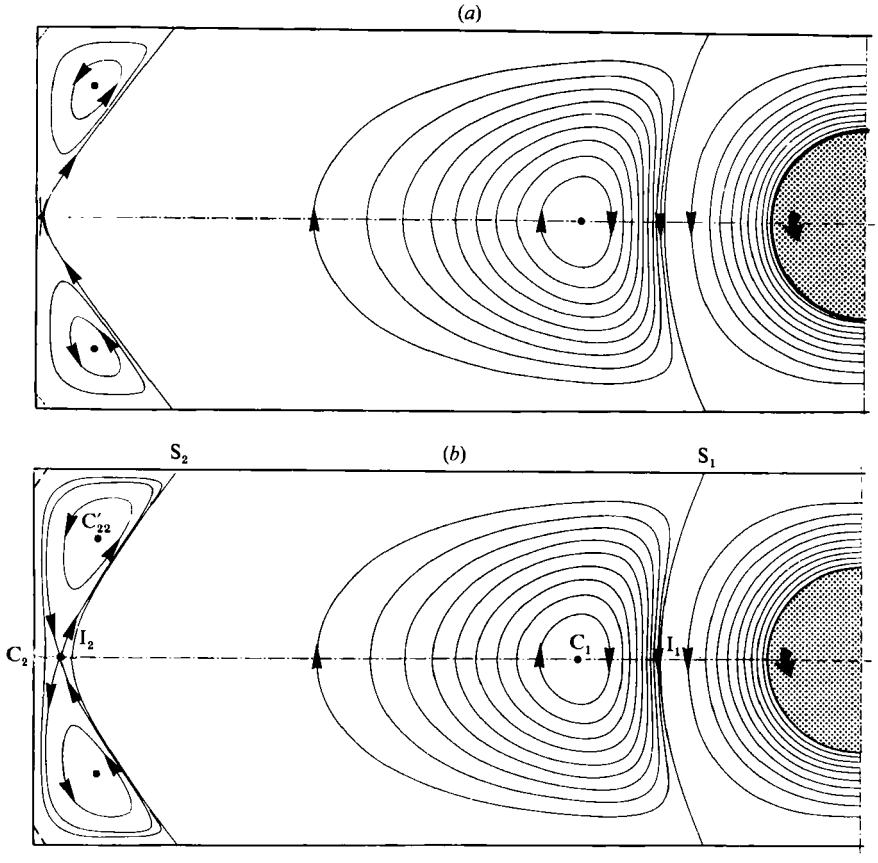

FIGURE 11. Formation of the second single-core cell from the new two-core one: (*a*) $A = 4.35$; (*b*) $A = 4.40$.

to adjust finally to a length of $2.80y_0$ which corresponds to the length of the reference cell, i.e. to the length of the cell which would be created in an infinitely long channel. Furthermore, both the numerical and experimental results confirm that the angle of separation of the cell dividing streamlines approaches the theoretical limit of 58.61° given by O'Neill (1983), when the aspect ratio becomes large; this is already well verified for the second dividing streamline from the value of A for which the first cell has reached its limiting structure i.e. for $A > 5.71$. However, the first dividing streamline, which remains influenced by the source of motion, namely the rotating cylinder, separates from the longitudinal walls with a greater angle (about 69°).

To complete our discussion on the periodicity of the cell formation, we have collected, in table 3, particular sequences of cell formation. We see, firstly, that the second coalescing process starts when the distance between the stagnation point C_1 of the previous cell and the endwall is equal to $2.80y_0$. Secondly, the aspect ratio which corresponds to each sequence of the formation of the second single cell (coalescing, merger, etc.) is obtained by the addition of the value of 2.80 to the aspect ratio that corresponds to the same sequence in the first single cell. Thus, we may conclude that the parameter $2.80y_0$ represents the aspect-ratio period of the formation of the successive single-core cells.

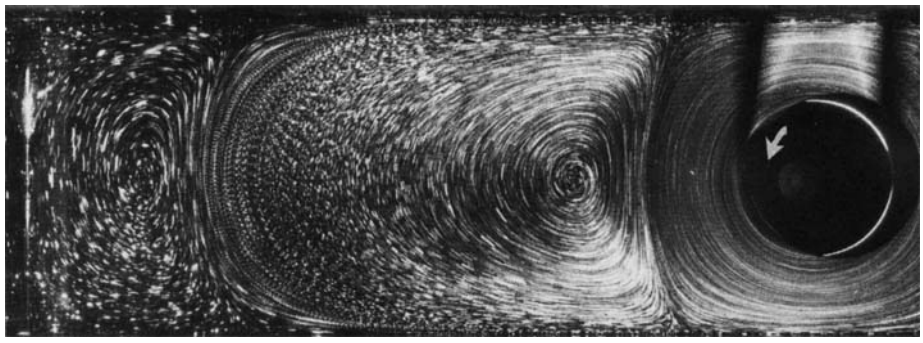

(*a*)

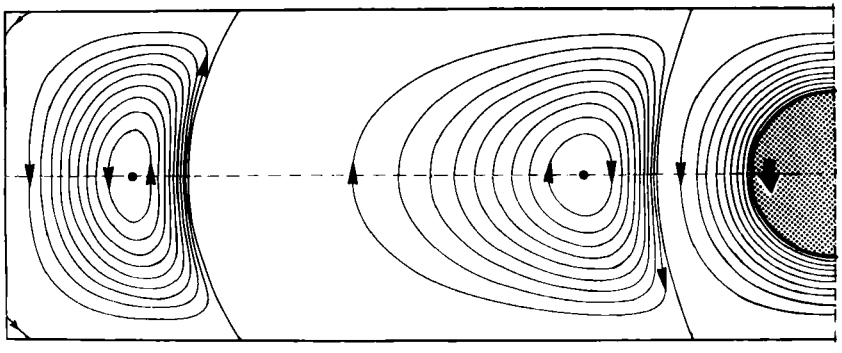

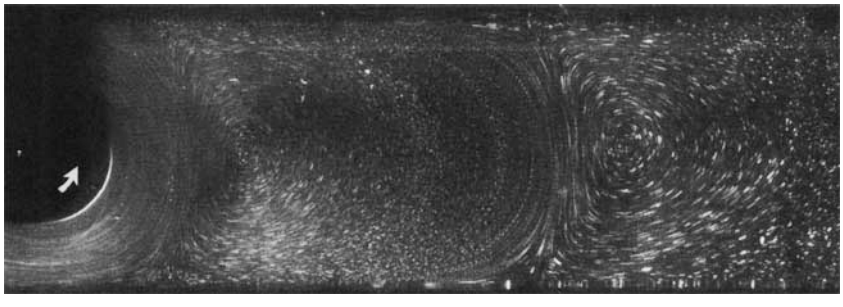

Limit of the hydrodynamic field visualized

(*b*)

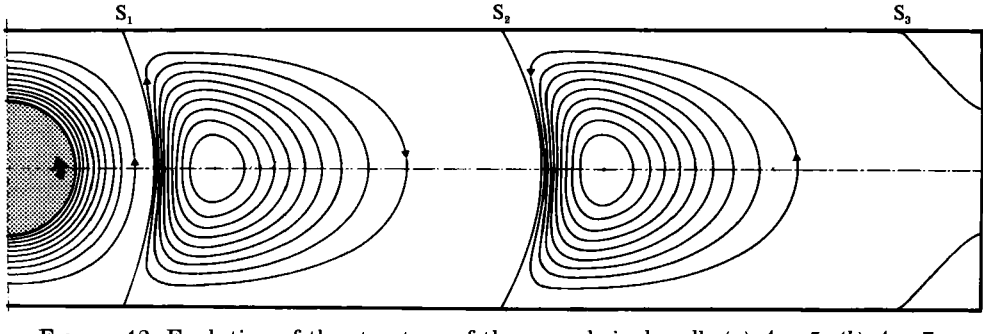

FIGURE 12. Evolution of the structure of the second single cell: (*a*) $A = 5$; (*b*) $A = 7$.

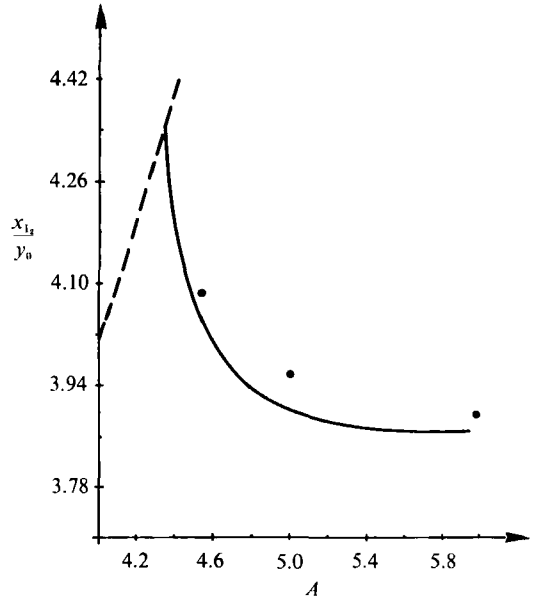

FIGURE 13. Location of the intersection I_2 of the second dividing streamline with the channel axis as a function of the aspect ratio: ——, numerical results; ●, experimental results; – – –, location of the endwall.

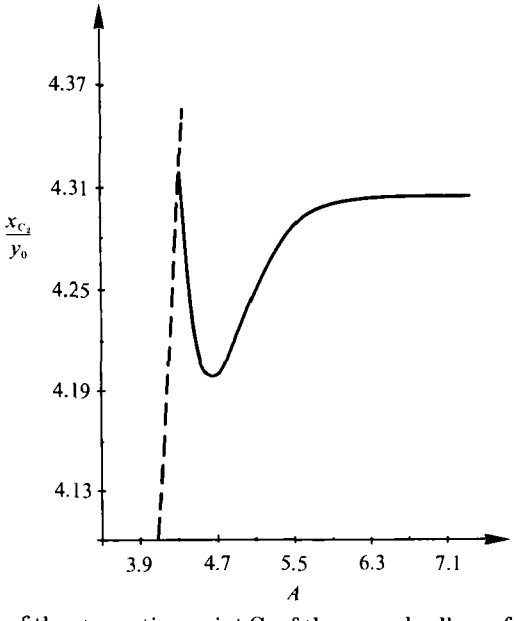

FIGURE 14. Location of the stagnation point C_2 of the second cell as a function of the channel aspect ratio: ——, numerical results; – – –, location of the endwall.

5. Conclusion

A low-Reynolds-number flow, driven by a rotating circular cylinder in a rectangular channel, has been analysed experimentally and numerically when the aspect ratio increases from 1 to 7, the main purpose being to determine the process

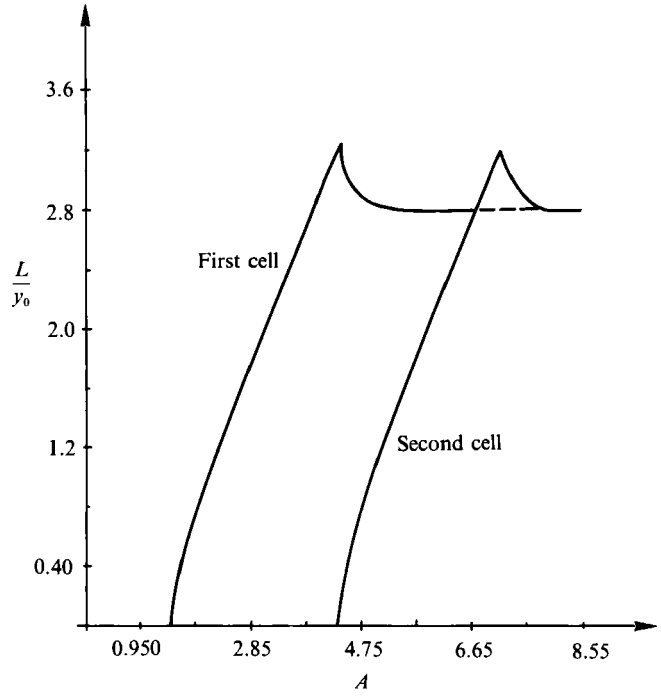

FIGURE 15. Evolution, as a function of the channel aspect ratio, of the length of the first and the second cells.

Sequence of events	A
Separation of the first dividing streamline from the endwall	1.50
Merger of the two first vortex core cells which leads to a single-core cell	1.80
The first dividing streamline reaches a limiting location of $1.07y_0$ on the flow axis	2.80
The axial stagnation point reaches a limiting location of $1.51y_0$	3.81
Separation of the second dividing streamline from the endwall; the length of the first cell is at a maximum, i.e. $3.27y_0$	4.34
Merger of a new main pair of vortex cores and formation of a second single-core cell	4.65
The second dividing streamline reaches a limiting location and consequently the length of the first single-core cell reaches its limiting value, i.e. $2.798y_0$	5.71
The stagnation point of the second single-core cell reaches a limiting location of $4.30y_0$ on the flow axis	6.62
Separation of the third dividing streamline from the endwall; the length of the second single-core cell is maximum, i.e. $3.23y_0$	7.10
The third dividing streamline reaches a limiting location and consequently the length of the second single-core cell reaches its limiting value, i.e. $2.792y_0$	8.5

TABLE 3. The main sequences of events in the process of formation of the first and second single-core cells with increasing aspect ratio

of formation of the successive cells which result. An excellent agreement between the numerical and experimental results has been found in all cases studied.

It has been shown how successive central cells form from the corners of the channel. Thus, when the aspect ratio increases from 1, the main corner cells grow

larger, coalesce and progressively merge into one single-core cell, which in turn grows longer as A increases. Then, when the distance between the stagnation point of this single-core cell and the endwall is equal to 2.80 times the channel width (y_0), a new pair of corner cells begins to coalesce; at this stage, the length of the previous cell is at a maximum. During this second coalescing process, the first cell contracts slightly to adjust finally to the structure of the reference cell, i.e. the cell which would set up in an infinitely long channel whatever the source of motion may be. A further increase of A provokes the development of a second single-core cell which evolves similarly to the first one. This periodicity has been proved both qualitatively and quantitatively. In fact, it has been found that every sequence in the cell formation repeats exactly when A increases with a step of 2.80. Consequently, knowledge of the detailed evolution of the first cell permits the structure of the flow for any other aspect ratio to be determined. The numerical results are given with an unusually high precision.

Complementary data concerning the flow evolution with the increase of the channel aspect ratio may be found in Hellou's (1988) thesis; they concern, in particular, velocity profiles, vorticity distribution on the channel walls, pressure on the rotating cylinder, the torque experienced by this rotating cylinder. Likewise, convincing comparisons with the results obtained by the authors quoted in our introduction, more especially with the results which concern the rectangular cavity, are given there and analogies shown.

Finally, the way the flow structure is progressively modified as the Reynolds number increases is under consideration and will be the subject of a future short paper.

The authors wish to thank Professor J. M. Bourot for originally suggesting the problem and his useful advice, as well as Professor S. C . R. Dennis for interesting discussions especially in view of a future numerical extension of the present calculation. We also thank Dr R. Bouard who helped us in the first phase of the experimental technique elaboration.

REFERENCES

Bouard, R. 1983 Etude de l'écoulement autour d'un cylindre soumis à une translation uniforme après un départ impulsif, pour des nombres de Reynolds allant de o à 10^4. Thèse de doctorat ès Sciences Physiques, Poitiers.

Bouard, R. & Coutanceau, M. 1986 Etude théorique et expérimentale de l'écoulement engendré par un cylindre en translation uniforme dans un fluide visqueux en régime de Stokes. *Z. Angew. Math. Phys.* **37**, 673–684.

Bourot, J. M. 1969 Sur l'application d'une méthode de moindres carrés à la résolution approchée du problème aux limites, pour certaines catégories d'écoulements. *J. Méc.* **8**, 301–322.

Bourot, J. M. 1984 Sur la structure cellulaire des écoulements plans de Stokes, à débit moyen nul, en canal indéfini à parois parallèles. *C. R. Acad. Sci. Paris* II **298**, 161–164.

Bourot, J. M. & Moreau, F. 1987 Sur l'utilisation de la série cellulaire pour le calcul d'écoulements plans de Stokes en canal indéfini: application au cas d'un cylindre circulaire en translation. *Mech. Res. Commun.* **14**, 187–197.

Buchwald, V. T. 1964 Eigenfunctions of plane elastostatics I. The strip, *Proc. R. Soc. Lond.* A **277**, 385–400.

Burgraff, O. R. 1966 Analytical and numerical studies of the structure of steady separated flows. *J. Fluid Mech.* **24**, 113–151.

Collins, W. M. & Dennis, S. C. R. 1976 Viscous eddies near a 90° and a 45° corner in flow through a curved tube of triangular cross-section. *J. Fluid Mech.* **76**, 417–432.

COUTANCEAU, M., BOUARD, R., BOUROT, J. M. & HELLOU, M. 1984 Sur la visualisation de la structure cellulaire de l'écoulement plan de Stokes engendré par la rotation d'un cylindre dans un canal. *C. R. Acad. Sci. Paris* II **298**, 767–770.

COUTANCEAU, M. & THIZON, P. 1981 Wall effect on the bubble behaviour in highly viscous liquids. *J. Fluid Mech.* **107**, 339–373.

DAVIS, A. M. J. & O'NEILL, M. E. 1977 Separation in a slow linear shear flow past a cylinder and a plane. *J. Fluid Mech.* **81**, 551–564.

DEAN, W. R. & MONTAGNON, P. E. 1949 On the study motion of viscous liquid in a corner. *Proc. Camb. Phil. Soc.* **45**, 389–394.

HASIMOTO, H. & SANO, O. 1980 Stokeslests and eddies in creeping flow. *Ann. Rev. Fluid Mech.* **12**, 335–363.

HELLOU, M. 1983 Etude theórique et expérimentale de l'écoulement plan de Stokes autour d'un cylindre en rotation dans un canal. Mise en évidence des courants secondaires et de leur structure cellulaire. Diplome d'études approfondies de l'Université de Poitiers.

HELLOU, M. 1988 Etude numérique et expérimentale de l'écoulement à structure cellulaire, engendré par la rotation d'un cylindre dans un canal. Thèse de l'Université de Poitiers.

HIGDON, J. J. L. 1985 Stokes flow in arbitrary two-dimensional domains: shear flow over ridges and cavities. *J. Fluid Mech.* **159**, 195–226.

JOSEPH, D. D. & STURGES, L. 1975 The free surface on a liquid filling a trench heated from its side. *J. Fluid Mech.* **69**, 565–589.

LEWIS, E. 1979 Steady flow between a rotating circular cylinder and fixed square cylinder. *J. Fluid Mech.* **95**, 497–513.

MAALOUF, A. & BOUARD, R. 1987 Etude de l'écoulement plan d'un fluide visqueux et incompressible autour et au travers de coques cylindriques poreuses, à faibles nombres de Reynolds. *Z. Angew. Math. Phys.* **38**, 522–541.

MEHTA, U. B. & LAVAN, Z. 1969 Flow in a two-dimensional channel with a rectangular cavity. *Trans. ASME* E: *J. Appl. Mech.* **36**, 897–901.

MOFFATT, H. K. 1964 Viscous and resistive eddies near a sharp corner. *J. Fluid Mech.* **18**, 1–18.

MOREAU, F. 1985 Sur la structure cellulaire des écoulements plans de Stokes, à débit moyen nul, en canal à parois parallèles. Diplome d'études approfondies de l'Université de Poitiers.

O'BRIEN, V. 1972 Closed streamlines associated with channel flow over a cavity. *Phys. Fluids* **15**, 2089–2097.

O'NEILL, M. E. 1983 On angles of separation in Stokes flows. *J. Fluid Mech.* **133**, 427–442.

PAN, F. & ACRIVOS, A. 1967 Steady flows in rectangular cavities. *J. Fluid Mech.* **28**, 643–660.

RYBICKI, A. & FLORYAN, J. M. 1987 Thermocapillary effects in liquid bridges. I. Thermocapillary convection. *Phys. Fluids* **30**, 1956–1972.

SANDERS, J., O'BRIEN, V. & JOSEPH, D. D. 1980 Stokes flow in a driven sector by two different methods. *Trans. ASME* E: *J. Appl. Mech.* **47**, 482–484.

SHEN, C. & FLORYAN, J. M. 1985 Low Reynolds number flow over cavities. *Phys. Fluids* **28**, 3191–3202.

SIGLI, D. 1970 Contribution à la mise au point d'une technique de résolution approchée du problème aux limites, pour un écoulement de révolution en régime de Stokes. Thèse de Doctorat de Troisième Cycle, Poitiers, France.

TANEDA, S. 1979 Visualization of separating Stokes flow. *J. Phys. Soc. Japan* **49**, 1935–1942.

WEISS, R. F. & FLORSHEIM, B. H. 1965 Flow in a cavity at low Reynolds number. *Phys. Fluids* **8**, 1631–1635.